Neuromethods (2012) 71: 23–39
DOI 10.1007/7657_2012_55

Published online: 17 May 2012

Mathematical Modeling and the Quantification of Brain Dynamics

Albert Gjedde and Dean F. Wong

Abstract

Neuroimaging greatly expanded the fundamental understanding of brain functions, and it has revealed novel treatment options in disciplines such as neurology, neurosurgery, and neuropsychiatry. The last 30 years have witnessed a flourish of approaches that include novel opportunities to image not only structure in ever-increasing resolution but also, and perhaps more importantly, the basic mechanisms of brain work that include the roles of regional cerebral blood flow and energy metabolism, neuronal network and neurotransmitter system activity, and most recently the abnormal deposition of amyloid-beta in brain tissue and the abnormalities of second messenger cascades that likely underlie important neuropathology.

The quantification of brain images is vital to the appropriate understanding and interpretation of these experimental and clinical findings. While many brain imaging agents, such as markers of amyloid-beta in dementia, are used with the ultimate goal of application to clinical prognostication and differential diagnosis, others will be fundamental research tools for understanding new drugs, such as antipsychotics, antidepressants, and anxiolytics, as well as drugs for relief of devastating neurological disorders such as multiple sclerosis, stroke, and dementia.

This chapter provides a brief introduction to some of the quantitative methods of understanding brain work and brain functions that neuroscientists developed in the last 30 years, and it highlights their importance to future tests of treatment. Here, an overall description of the basic elements of quantification, and, in particular, mathematical modeling of dynamic brain images, is presented both to justify the role of such modeling in initial study development, and to validate specifications for use in clinical settings. Quantification and kinetic modeling are just as important as image reconstruction and structural identification of regions of interest, and they are fundamental components of all new brain imaging tools. The quantitative methods presented in this brief introduction continue to underpin the routine approaches and hence matter to most clinicians and clinician scientists involved in brain imaging.

Key words: Binding potential, Clearance, Kinetics, Neuroimaging, Quantitative analysis, Neuroreceptor mapping

1. Introduction

Since the inception of molecular imaging of living brains, a major challenge for both clinicians and investigators has been the quantification of the images. Originally, brain images, by default, were anatomical, with a semiquantitative component of brain tumor size

or degree of midline shift for mass effect, or evidence of stroke. Later, as images acquired a functional component when active and passive conditions were compared, the challenge became to convincingly add numerical outcome measures to the qualitative nature of functional neuroimaging. This chapter outlines the general principles of brain image quantification as they relate to brain function. We review a common analytical approach that provides both an understanding of current findings and, in response to ever more complex brain imaging methods, a progression of improvements to quantification. For a more detailed treatment, consult the textbook *Neurokinetics* (1).

From the introduction of early single-photon imaging with radioactive gasses in the 1950s to the arrival of positron tomographic imaging of cerebral blood flow (CBF) and the cerebral metabolic rate for glucose (CMR_{glc}) in the late 1970s and early 1980s, models have been the backbone of quantification in functional imaging. Indeed, without quantification through modeling, images of CBF and CMR_{glc} were meaningless (although nonquantitative regional measures still play a role in some studies of brain activation). The advent of neurotransmitter and receptor imaging in 1983 necessitated even more sophisticated models of separation of specific from nonspecific binding of radiolabeled ligands or drugs, which required multiple measurements of neurotransmitter action in the synapse and in the extracellular space following brain activation. Thus, with so many opportunities for functional brain mapping of correlates of neuroanatomy and neurotransmission, it is essential that appropriate mathematical models be formulated and, of course, validated. Fortunately, the many aspects of functional brain imaging can be explained with the few basic principles outlined below.

The quantification of brain images has undergone an impressive evolution, from the advent of functional mapping of blood flow to the most complex mapping of second and third messenger responses to neurotransmission. The acquisition of images by means of appropriate instrumentation, such as positron emission tomography (PET) or MR, is the important first step of the quantification. The recording often results in a dynamic series of images, although simplified procedures also exist for added clinical practicality. The final step is the assignment of quantitative values to neurobiological processes relevant to specific brain regions. In some cases, the regional assignment can be driven by known neuroanatomical subdivisions such as regions (ROI) or volumes (VOI) of interest, or, alternatively, by clusters of volume elements (voxels) selected by independent Statistical Parametric Mapping (SPM) methods that refer to the effects of specific phenomena or stimuli in places commonly assumed to represent networks of collaborating neuronal ensembles and brain regions. Regardless of the approach, the assignment always depends on some form of a quantitative model.

In this chapter, we focus on the assignment of physiological values, be they measures of blood flow or concentration of receptor, or transporter, proteins per unit volume of brain tissue.

2. The Concept of Models

By definition, a model is a simplification of the actual physiological process. In the case of quantification of brain function, two approaches are common. They include the widely used "compartmental" model as well as the less known but relevant "non-compartmental" model. As the latter mostly applies to more esoteric measurements, such as the assessment of the inhomogeneity of blood flow rates (e.g., (2)), we limit our discussion to the more traditional and better tested compartmental model.

2.1. Definition of Compartments as Tracer States

A compartment has a specific mathematical definition, and a model is a set of compartments that simulates a biological system. Compartmental analysis tests the validity of the model of the combined kinetic behaviors of the elements of each compartment, and the model provides a basis for prediction of subsequent behaviors. Thus, the model is the mathematical hypothesis of the dynamics of a biological system, and the compartmental analysis is the test of predictions generated by this hypothesis. Sheppard (3) defined compartments as quantities of a tracer or its metabolites, the concentrations of which remain the same "everywhere," each quantity having a single state that may vary in time but not in space. A quantity is the number of molecules in units of mol (6.02×10^{23}). Subsequently, Rescigno and Beck (4, 5) modified Sheppard's definition of a compartment to refer to a tracer state that varies specifically in time as prescribed by the expression

$$\frac{\mathrm{d}m}{\mathrm{d}t} = j - km \tag{1}$$

where m is the quantity (mol) of tracer that belongs to the compartment (i.e., has the relevant state), k the relaxation (or "rate") constant, and j the flux of tracer molecules into the compartment as a function of time. It follows from this definition that the relaxation constant is given by the relationship

$$k = \frac{j}{m} - \frac{1}{m}\left(\frac{\mathrm{d}m}{\mathrm{d}t}\right) \tag{2}$$

where, at steady-state, when $\mathrm{d}m/\mathrm{d}t = 0$, k is the turnover rate j/m. The definition refers to a situation in which the escape of tracer from the particular state (i.e., the "relaxation" of the state) is a first-order process. Whether or not this requirement is met depends on the process responsible for the relaxation.

The more compartments a model has, the less it discriminates between the measured biological parameters, although the model description of the observed data may be of practical value as an operational account of events. In addition, the relaxation constants, or transfer coefficients, of a series of compartments can be distinguished only when their magnitudes are not too different. Slow relaxations tend to obscure rapid relaxations as the compartments move towards a secular equilibrium. Thus, by analyzing the organ uptake of a tracer as a function of time, only a limited number of compartments and transfer coefficients can be identified. In transient analysis, the independent and dependent variables are measured as functions of time and the desired coefficients are estimated from the fundamental solution by regression analysis using computerized optimization. The solution to the equations above is the prototype of an operational equation used for regression analysis in which the input (j) and output (m) functions are compared to yield the value of the parameter k which "optimizes" the comparison:

$$m(T) = \mathrm{e}^{-kT}\left[m(0) + \int_0^T j(t)\mathrm{e}^{-kt}\,\mathrm{d}t\right] \tag{3}$$

where the parameter k of unknown magnitude is assigned a property of biological interest. The results of regression analysis cannot always be related to the biological characteristics of the system, however. In such cases, the regression analysis is meaningful only when the validity of the model is independently established. Usually it is impossible to decide the validity of the model and obtain the best estimates of the parameter at the same time. Mathematical simulation of the behavior of the model together with actual experimental verification helps justify the choice of the model.

Compartments are idealized descriptions of the actual physiological processes and build on a number of fundamental assumptions that include uniform distribution of molecules, endogenous as well as exogenous (introduced as tracers of native molecules such as glucose). These assumptions are not actually fulfilled, but reality is sufficiently close to allow useful results to emerge from the modeling. Commonly, in quantification of compartmental models of brain function by means of PET or SPECT, the intravenously administered radiopharmaceutical passes from the vascular space (first compartment) across the blood–brain barrier (BBB) into compartments of the brain tissue. For CBF measurements, the brain often is assumed to hold a single well-stirred compartment; for oxygen consumption measurements, the brain tissue proper is assumed to be a single compartment (second compartment); and, for measurements of glucose metabolism or neuroreceptor binding potentials, additional compartments are thought to exist, including third and fourth compartments in the case of receptors accounting for populations

Table 1
Parameters of biological interest

Basic neurobiological variables	Symbol	Units
Cerebral blood flow	F	ml/100 g/min
Cerebral metabolic rate for oxygen	CMR_{O_2}	μmol/100 g/min
Cerebral metabolic rate for glucose	CMR_{glc}	μmol/100 g/min
FDOPA conversion to fluorodopamine	k_3 K_{in}	min^{-1} ml/100 g/min
Receptor density	B_{max}	pmol/g
Binding potential or receptor availability	BP_{ND}	Ratio
Receptor half-saturation or Michaelis constant	K_D	pmol/ml

of nonspecifically and specifically bound radioligand molecules. Combinations of transporter, enzyme, and receptor compartments further complicate the models.

Regardless of the model of specific brain dynamics, the goal of the model is ultimately to link the compartments and to describe the links in the forms of mathematical equations. The equations are used to extract the relevant parameters, such as the clearance of tracer molecules from the circulation to brain tissue across the BBB (K_1), the rate constant of efflux from the brain tissue back to the vascular space (k_2), the rate of binding to receptors in brain (k_3), and the rate of dissociation (k_4). Biological variables of physiological or pathophysiological interest, such as the absolute rate of CBF, are linked to these model parameters separately or in combination (Table 1). For example, in measures of blood–brain transfer coefficients, the initial or unidirectional clearance parameter K_1 equals the product of the fraction of unidirectional extraction (E) of the radiotracer and the rate of blood flow (F). In the case of receptor binding, the ratio k_3/k_4 is the binding potential, an index of empty receptors available for binding that is proportional to the ratio of the maximum number of receptors that can be occupied, to the Michaelis–Menten relaxation constant, B_{max}/K_d. Thus, the goal of the analysis is to estimate the model parameters that link the compartments and combine them to form the ultimate biological variables of interest.

2.2. Determination of Parameters

The challenge is to obtain unbiased estimates of parameters, of which some are rate constants and some are volumes that together form clearances. Researchers typically obtain dynamic records at

specific time points, as PET or SPECT images, of the fraction of the radiopharmaceutical that traverses from the capillary portion of the vascular space through the brain tissue with the relevant receptor, enzyme, or transporter sites and back to the circulation. The dynamic time vs. radioactivity data are then compared with the predictions made from specific compartmental models by solution of the applicable nonlinear differential equations. The resulting parameter estimates are those that optimize the match of the predictions to the dynamic records. The magnitudes of biological variables, such as CBF, glucose and oxygen metabolic rates, and receptor availability, are then the results of combining the parameter estimates as dictated by the mathematical analysis of biological processes.

2.3. Specific Examples of Quantitative Modeling of Tracer Uptake in Brain

2.3.1. Single Compartment Modeling

A single compartment describes the uptake and distribution of a labeled or detectable tracer when it encounters no barriers to its instant and even pervasion of the entire brain volume. In such a case, only blood flow limits the uptake, distribution, and subsequent removal of the substance from the brain volume, and blood flow rates ideally can be deduced from the behavior of the tracer. Once the tracer enters the brain, the single compartment solution to the differential equations predicts the instant and unlimited distribution of the labeled blood flow tracer in the entire brain space, according to the equation (6)

$$M^*(T) = F\int_0^T C_a^*(t)e^{-F(T-t)/V}\,dt \qquad (4)$$

where $M^*(T)$ is the tracer quantity in brain at the time T after administration, F is the blood flow rate, $C_a^*(t)$ is the arterial concentration of the tracer, and V is the steady-state volume of distribution of the tracer in the entire brain volume. The problem is that very few tracers match the ideal requirements for single compartment modeling.

Example: Determination of CBF

The measurement of blood flow rates and their functionally stimulated changes in the brain is a classic approach to functional brain mapping (7). In the earliest application of the approach, inhalation of a measurable tracer such as nitrous oxide, according to the methods of Kety and Schmidt (8) or Raichle et al. (9), allowed measurements to be completed in humans, and the methods superseded the autoradiography of animal brains ex vivo, in which a single injection and the subsequent circulation of the tracer are terminated by sacrifice of the animal and removal of the brain. The equivalent event in humans is the end of image acquisition, and the general approach has been validated in numerous studies of what are now standard methods of blood flow measurement. Although a number of different applications of the methods are available, regional mapping of the blood flow variable requires

arterial blood sampling for the mathematical extraction of the tissue's characteristic impulse response function from the input and output time–activity curves. The input function is thus the key to compartmental modeling as the determining function of differential equations that forces the uptake into the single brain compartment. Only few tracers, such as labeled butanol and antipyrine, are fully diffusible to the extent that they fulfill this requirement, while a more common tracer such as radiolabeled water is less diffusible and consequently requires additional compartments to fully and accurately account for radiolabeled water remaining in the bloodstream (10).

2.4. Dual Compartment Modeling

Two compartments describe the uptake and distribution of a labeled or detectable tracer, when the tracer encounters only one significant barrier to its instant and even pervasion of the brain volume. The effect of the barrier is to delay the distribution as well as to generally expand the steady-state volume of distribution, depending on the properties of the barrier, which can be any one of a number of obstacles to unlimited pervasion, including membrane transporters, receptors, and enzymes. In this case, not only blood flow but also the transport, binding, or metabolism of the tracer limit the uptake, distribution, and subsequent removal of the substance from the brain volume, the kinetics of which in the most ideal of cases can be deduced from the behavior of the tracer,

$$M^*(T) = V_0 C_a^*(T) + K_1 \int_0^T C_a^*(t) e^{-K_1(T-t)/V_c} \, dt \qquad (5)$$

where the relative magnitudes of K_1 and V_c determine whether or not any loss of tracer will be evident during the time of observation. When K_1 is very small compared to V_c, or V_c very large compared to K_1, the equation reduces to the expression of irreversible trapping of the tracer in the brain tissue,

$$M^*(T) = V_0 C_a^*(T) + K_1 \int_0^T C_a^*(t) dt \qquad (6)$$

which linearizes to the equation for the Gjedde–Patlak, or slope–intercept, plot (11),

$$\frac{M^*(T)}{C_a^*(T)} = V_0 + K_1 \int_0^T \frac{C_a^*(t)}{C_a^*(T)} dt \qquad (7)$$

where V_0 is the ordinate intercept and K_1 the slope. This is the original formulation of the plot for determination of blood–brain transfer of substances across the BBB that is applicable in principle to uptake across any single barrier.

2.4.1. Example: Determination of Cerebral Oxygen Consumption ($CMRO_2$)

Oxygen is subject to reduction by the cytochrome a,a3 enzyme in the mitochondria of brain cells, in which the oxygen rapidly is converted to water. This allowed early users of PET to argue that brain tissue has only two compartments of labeled molecules, oxygen bound to hemoglobin in the circulation, and water of metabolism in the tissue (12). Measurements of oxygen consumption with oxygen-15-labeled oxygen are therefore among the first applications of PET in which the uptake and removal of labeled molecules are predicted by the dual compartment solution to the two differential equations describing the oxygen reduction reaction and the subsequent exodus of the labeled water (13). When V_0 is the volume of distribution of oxygen in the vascular compartment of the brain, relative to the arterial concentration, $K_1 \equiv \mathrm{CMRO_2}/[\mathrm{O_2}]$ is the initial clearance of the oxygen from the vascular compartment that is coincident with the conversion to water of metabolism, relative to the oxygen concentration in arterial blood, and $k_2 \equiv K_1/V_e$ is the rate of removal of the water from the exchange volume V_e.

2.4.2. Triple Compartment Modeling

Three compartments describe the uptake and distribution of a labeled or a measurable tracer when multiple barriers delay the pervasion of the entire brain volume, including for example two membrane transport steps or a membrane transport step and a receptor binding or enzyme reaction step. The properties of the third compartment in relation to the duration of observation determine the extent to which the third compartment is kinetically detectable. They also determine whether the labeled molecules are more or less trapped in the third compartment. The variably reversible accumulation of metabolites provides several opportunities for quantification of the uptake by means of a wealth of different solutions of the underlying differential equations (1), with or without dynamic recording of the uptake in the brain, using such tracers as [^{11}C]glucose, 6-[^{18}F]fluorodeoxyglucose (FDG), or [^{18}F]fluorodihydroxyphenylalanine (FDOPA). The total radioactivity is a rather complex formula that incorporates all of the rate constants defining the three compartments,

$$M^*(T) = V_0 C_a^*(T) + K_1 \left[\left(\frac{q_2 - [k_3 + k_4]}{q_2 - q_1} \right) \int_0^T C_a^*(t) e^{-q_2(T-t)}\, dt + \left(\frac{q_1 - [k_3 + k_4]}{q_2 - q_1} \right) \int_0^T C_a^*(t) e^{-q_1(T-t)}\, dt \right] \quad (9)$$

where

$$2q_1 = k_2 + k_3 + k_4 - \sqrt{(k_2 + k_3 + k_4)^2 - 4k_2k_4}$$

$$2q_2 = k_2 + k_3 + k_4 + \sqrt{(k_2 + k_3 + k_4)^2 - 4k_2k_4}$$

and k_3 and k_4 are the rate constants of entry into and exit from the third (or "inner") compartment, and are descriptive of the processes that define entry and exit. The processes can be any physical or biochemical step that delays the further pervasion of the labeled molecules, including passive or facilitated diffusion, active transport, and binding or enzyme reaction. In some cases, molecules enter but cannot subsequently exit the third compartment that then acts not only as a sink but also as a trap, at least for some period of time. In those cases, the rate constant k_4 essentially is zero compared to the remaining rate constants, and the total quantity of labeled compound in the tissue is given by the equation first derived by Sokoloff et al. (14),

$$M^*(T) = V_0 C_a^*(T) + K_1 \left[\left(\frac{k_2}{k_2 + k_3} \right) \int_0^T C_a^*(t) e^{-(k_2+k_3)(T-t)} \, dt + \left(\frac{k_3}{k_2 + k_3} \right) \int_0^T C_a^*(t) \, dt \right] \quad (10)$$

which eventually linearizes to a form that extends the multitime graphical analysis or slope–intercept plot beyond the initial barrier discussed above to the process of trapping in the third compartment, depending on the magnitudes of k_2 and k_3, as first presented by Gjedde (15),

$$M^*(T) \cong \left(\frac{K_1 k_2}{[k_2 + k_3]^2} \right) C_a^*(T) + K_1 \left(\frac{k_3}{k_2 + k_3} \right) \int_0^T C_a^*(t) dt \quad (11)$$

where $V_g \equiv K_1 k_3/(k_2 + k_3)^2$ is an apparent precursor volume of distribution, and $K \equiv K_1 k_3/(k_2 + k_3)$ is the net clearance of the tracer into the trap, which is measurable by linear regression, when the magnitudes of the rate constants have established the steady state of the second or "outer" compartment (15, 16),

$$\frac{M^*(T)}{C_a^*(T)} \cong V_g + K \int_0^T \frac{C_a^*(t)}{C_a^*(T)} dt \quad (12)$$

where V_g is the ordinate intercept and K is the slope. It is evident that (12) bears a superficial resemblance to (7), but the parameters of the linear regression are different.

Example I: Determination of Cerebral Glucose Metabolism (CMR_{glc})

The measurement of brain glucose metabolism is based on the use of radiolabeled derivatives of native glucose as the precursor of glucose phosphorylation. The first compartment is the radiolabeled glucose analog in the vascular compartment of the brain. Of the glucose analog delivered to the brain circulation, only a small fraction (~10 %) crosses the BBB and enters the brain tissue where it forms the second compartment. About half of the glucose analog is then converted by the hexokinase enzyme step into the labeled metabolite product of the phosphorylation where it is trapped for

some period of time (1, 14–17). A quantitative map of regional glucose metabolism can be obtained as a single image 45–90 min after injection of the radiotracer. The transporters of glucose and enzymes of glucose metabolism express different affinities to glucose analogs and therefore leave different amounts of precursor and metabolite, which must be accounted for by an isotopic factor, the so-called lumped constant, a variable defined as the ratio of the net extraction fractions of the glucose analog and native glucose, which has been measured, tabulated, and reinterpreted in numerous studies (18, 19). The lumped "constant" actually varies in abnormal situations, but can be assessed separately with full dynamic modeling (20).

Example II: Determination of FDOPA Metabolism (K_{in} and k_3)

Garnett et al. (21) first visualized the conversion of DOPA to dopamine in the human brain by labeling DOPA with fluorine-18 as ^{18}F-DOPA (FDOPA) and obtaining early PET images of the trapping of the tracer as fluoro-dopamine in the vesicles of the presynaptic dopaminergic terminals, which were primarily visible in the striatum. The modeling of the uptake of FDOPA posed special problems, as it includes an additional compartment, defined by the conversion of FDOPA to 3-*O*-methyl-FDOPA both inside and outside the brain tissue, and the subsequent efflux of the methylated product from brain tissue. Use of the linearization of the slope–intercept plot nonetheless became popular as a measure of net clearance, commonly symbolized as K_i in reports of FDOPA uptake, originally due to a misprint of the term K_{in}. The resulting values of K_i did not, however, directly apply to any known flux, because DOPA unlike glucose in healthy volunteers originates in brain tissue and not in circulation. This shortcoming stimulated the search for modeling approaches that yielded estimates of the rate constant of trapping k_3 and, in later treatments, also the efflux or turnover constant k_{loss} (22, 23).

Example III: Determination of Receptor Availability (k_3 and BP_{ND})

Wagner et al. (24) first visualized the binding of an exogenous radioligand to dopamine D_2-like receptors (D_{2-3} or D_{2-4}) in the human brain, and they subsequently found that the binding declines with age (25, 26). The quantification of the binding necessarily depended on the reversibility of the radioligand's binding that reflects the affinity of the receptor for the ligand, which in turn depends largely on the rate of dissociation of the ligand from the receptor. The earliest analysis of binding addressed the uptake of the radioligand *N*-[^{11}C]methylspiperone (NMSP), towards which the D_2-like receptors have such a high affinity that the binding essentially is irreversible in the period available for tomography. The binding is hence subject to modeling according to (10) rather than (9) (27, 28), but regression of observations to (10) yields an estimate of k_3 as a function of the number of receptors available for binding. Blockade of receptors with an endogenous or exogenous competitor (Fig. 1) served to reduce the magnitudes of both K and

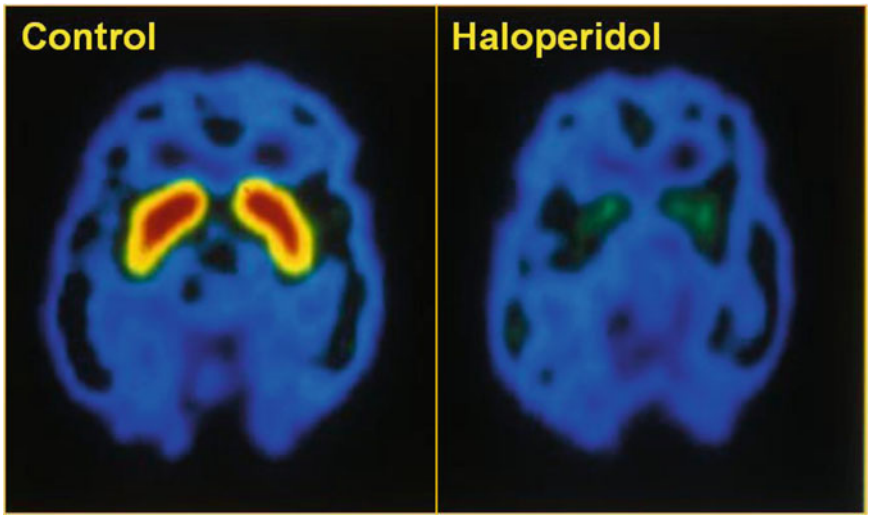

Fig. 1. Receptor blockade study using *N*-[^{11}C]methylspiperone and haloperidol as a blocker of D_2-like dopamine receptors (27, 28).

k_3 according to (11) and (12) (29). However, calculation of absolute receptor numbers was not possible without separate knowledge of the magnitude of the receptor dissociation rate constant k_4.

The ratio of the rate constants k_3 and k_4 is the ratio of bound to unbound ligands, also known as the bound-to-free (B/F) ligand ratio of the Scatchard and Eadie–Hofstee receptor plots, also introduced as the binding potential (BP_{ND}), relative to the unbound or non-displaceable ("ND") tracer, or receptor availability index (30). Estimates of association and dissociation rate constants and their ratio (the binding potential) were only obtained after introduction of radioligands with rapidly reversible binding due to the somewhat lower affinity of the receptors towards these ligands, exemplified by [^{11}C]raclopride (31). The greater reversibility then requires modeling by means of (9), which in specific cases of particularly rapid binding reduces to (5) where V_{e} is then replaced by V'_{e} such that, at steady state, $V'_{\mathrm{e}} = K_1/k'_2 = K_1/k_2(1 + (k_3/k_4)) = V_{\mathrm{e}}(1 + \mathrm{BP_{ND}})$ (32). The exchange volume still determines the steady-state uptake in regions of the brain with no expansion of the exchange volume by specific binding. Inspired by early attempts to determine bound-to-free ratios in animals in vivo (33), at steady state, it is now common to determine the binding potential as a simple function of the ratio between the quantities of tracer in the binding and nonbinding regions, $\mathrm{BP_{ND}} = [V'_{\mathrm{e}}/V_{\mathrm{e}}] - 1 = \left[M^*_{\mathrm{VOI}}/M^*_{\mathrm{ND}}\right] - 1$, where VOI refers to a VOI with binding, and ND as above refers to a volume of non-displaceable tracer uptake because of absent saturable binding, as is of course also implied by the "bound-to-free" ratio term.

Example IV: Determination of Receptor Binding Capacity (B_{max})

Presented as the B/F ratio term, the binding potential is a complex entity; the determination is simple but the interpretation is difficult, as it depends on the concentrations in the right place of at least two ligands, the endogenous ligand itself and the exogenous tracer used in the experimentation, as well as on the affinities of all the relevant receptors towards both ligands. Because there are a number of compartments where the concentration of the exogenous ligand can be probed, there is more than one binding potential term in use by different applications, including the aqueous concentration (BP_F) and concentrations relative to whole-blood or plasma (BP_P) or to the whole brain tissue volume in question (BP_{ND}) (34), the last of these equal to the original formulation, which is also the most relevant to the use of Scatchard or Eadie–Hofstee plots. Scatchard and Eadie–Hofstee plots are linearizations of the relationship between the quantity of bound ligand at different concentrations and the binding potential,

$$B = B_{max} - [V_d K'_D][BP_{ND}] \quad (13)$$

where B is the quantity of bound ligand, B_{max} is the maximum binding capacity, and V_d is the volume of distribution of the radioligand to which the Michaelis half-saturation constant K'_D refers, as affected by the concentration of an additional inhibitor in the form of an exogenous inhibitor or the endogenous dopamine, itself, or the radioligand at low specific activity. However, the exogenous ligand is not a tracer in the classical sense if the concentration measurably occupies the receptor and lowers the number of unoccupied receptors (Fig. 2). The binding relations must be in steady state to allow the terms of this rearrangement of the Michaelis–-Menten equation to be valid, but there really is no guarantee that the

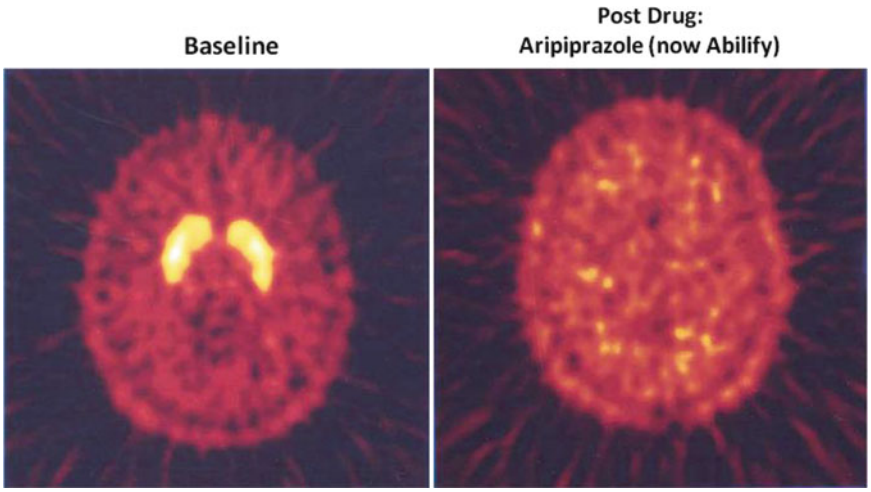

Fig. 2. [^{11}C]raclopride brain positron emission tomography (PET) images of dopamine D_2-like receptors before and after a 14-day treatment with 30 mg/day of aripiprazole (46).

magnitudes of B_{max} and K'_D will remain true constants when the receptors are occupied by exogenous ligand molecules at pharmacologically active doses. Nonetheless, this is the common assumption underlying the use of blockade by an unlabeled inhibitor with irreversible PET radiotracers (such as (28) or (35)), as well as when reversibly binding radioligands with different specific activities are used to determine affinity, and maximum binding capacity, of neurotransmitter receptors (36).

3. Mapping Neuroreceptors at Work

Interventions or changes of brain states that affect the release and concentration of endogenous neurotransmitters, without directly influencing the receptors, are known to affect the binding of radioligands at tracer doses, as reflected in the calculated magnitudes of the binding parameters B_{max} and K'_D. Equation (13) can be rearranged to show all the terms that affect the magnitude of the binding potential,

$$[BP_{ND}] = \frac{B_{max}}{V_e C_a + V_d K_D \left(1 + \frac{C_I}{K_I}\right)} \tag{14}$$

where C_a is the arterial concentration of the tracer ligand, V_e its exchange volume, K_D the Michaelis half-saturation constant of the tracer ligand, C_I the concentration of a competing endogenous ligand, and K_I the half-inhibition constant of the competing endogenous ligand. If an intervention or a change of a brain state affects the binding potential of the tracer ligand without seemingly affecting the maximum binding capacity of the receptors, exchange volume, distribution volume, or affinity of the receptors towards the exogenous ligand, then a change of the concentration or inhibitory constant of an endogenous competitor commonly is inferred,

$$\frac{C_I}{K_I} = \frac{B_{max}}{[V_d K_D][BP_{ND}]} - \left(\frac{[V_e C_a]}{[V_d K_D]} + 1\right) \tag{15}$$

the magnitude of either of which in principle is calculable from (15) by subtraction. For a change of concentration it takes the form

$$\frac{\Delta C_I}{K_I} = \frac{B_{max}}{[V_d K_D]} \left(\frac{BP^b_{ND} - BP^c_{ND}}{BP^b_{ND} BP^c_{ND}}\right) = \frac{BP^a_{ND}}{BP^b_{ND}} \left(\frac{BP^b_{ND}}{BP^c_{ND}} - 1\right) \tag{16}$$

where the superscripts a, b, and c refer to binding potentials in the absence of any occupier (a), at the experimental baseline (b), and in the experimental condition (c), i.e., the latter two before and after the intervention or change of brain state. The result in the bracket $\left([BP^b_{ND}/BP^c_{ND}] - 1\right)$ often is reported as the fractional transmitter

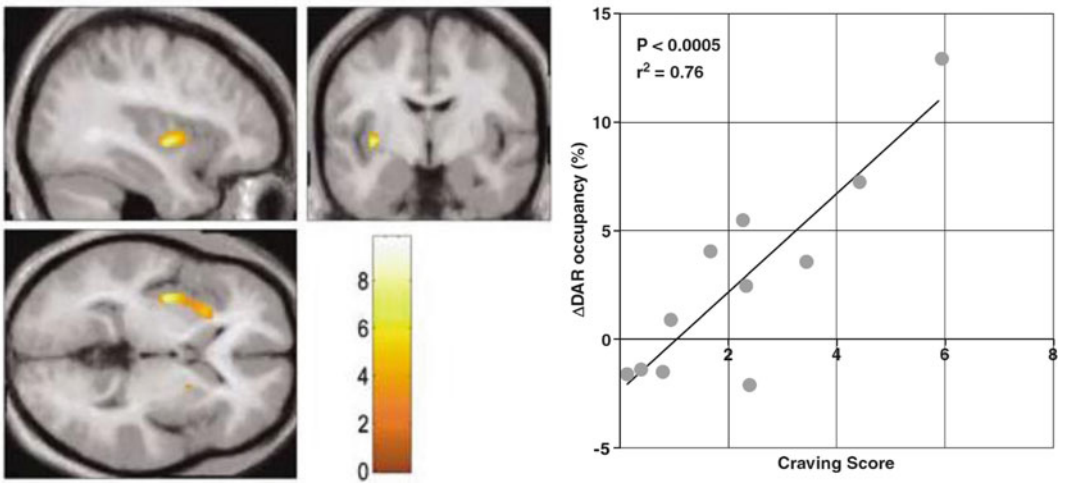

Fig. 3. [^{11}C]Raclopride PET with a craving cue. Patients with cocaine abuse were given two consecutive PET scans, with a neutral cue during the baseline PET and craving cue during the second PET. Then, Statistical Parametric Mapping (SPM) was used to look for regions of significant change in occupancy. *Left panel*: SPM generated map showing a cluster in the left anterior putamen where increased release of endogenous dopamine in response to a craving cue correlated with craving score. *Right panel*: Scatterplot and regression analysis of the percent change in DAR occupancy with craving score for the cluster shown in the SPM map (39).

"release," although the magnitude depends on transmitter occupancy in the baseline, and actual release is but one of several possible interpretations. Evidence of "release" has been reported for dopaminergic neurotransmission in a number of situations, the most commonly studied being the effect of amphetamine administration, as well as with non-pharmacological intervention in the form of exposure to neuropsychological stimuli of different individuals (37, 38), including former cocaine addicts experiencing renewed craving upon presentation of cocaine "cues" (39) as illustrated in Fig. 3. Some of the reported changes differ in healthy volunteers and patients with neuropsychiatric disorders (40, 41). Evidence of release has also been reported for other transmitter systems, including noradrenergic neurotransmission (42) and the opioid system (43, 44). The approach also applies to transmitter depletion as in the case of α-methyl-*p*-tyrosine inhibition of dopamine synthesis when the relevant binding potentials actually increase (45).

4. Challenges to Quantification

Currently, a major challenge to quantification is the incomplete and still improving art of nonlinear regression analysis of model-based convolution results to observed data; progress on this front could improve and simplify computation. The observed data itself is affected by the stochastic nature of brain images in which the signal

is smeared across a certain three-dimensional volume due both to the physical process of dual-photon generation and the partial volume effects of the tomography. These factors introduce considerable noise into the data and hence uncertainty into the estimates of the equation parameters.

For good reasons, this chapter does not address future challenges to quantification, including corrections for the finite resolution of instruments (such as the partial volume effects), lack of fully specific radiopharmaceuticals (such as radiotracers that bind to multiple sites), and metabolisms of the radiotracer. Apart from these concerns, however, this chapter has served to give a general overview of mathematical modeling approaches to functional brain imaging with PET or SPECT, in particular, while we wait for other modalities as well as for more and more challenging and exciting developments of functional brain imaging to emerge.

Acknowledgements

Global Excellence Award 2010, Capital Region, Denmark (Gjedde). NIH-NIDA midcareer award K24 DA000412 (Wong). Special thanks for technical assistance to Ayon Nandi, MS; and Rebecca Mellinger-Pilgram, BS, Johns Hopkins University.

References

1. Gjedde A, Bauer WR, Wong DF (2011) Neurokinetics: The dynamics of neurobiology in vivo. Springer, New York
2. Kuikka JT et al (1991) Mathematical modelling in nuclear medicine. Eur J Nucl Med 18 (5):351–362
3. Sheppard CW (1948) The theory of the study of transfers within a multi-compartment system. J Appl Phys 19(70)
4. Rescigno A, Beck J (1972) Compartments. In: Rosen R (ed) Foundations of mathematical biology, 1st edn. Academic, New York, pp 255–322
5. Rescigno A, Beck JS (1987) The use and abuse of models. J Pharmacokinet Biopharm 15 (3):327–344
6. Gjedde A (1980) Rapid steady-state analysis of blood-brain glucose transfer in rat. Acta Physiol Scand 108(4):331–339
7. Gjedde A (2008) Functional brain imaging celebrates 30th anniversary. Acta Neurol Scand 117(4):219–223
8. Kety SS, Schmidt CF (1948) The nitrous oxide method for the quantitative determination of cerebral blood flow in man; theory, procedure and normal values. J Clin Invest 27 (4):476–483
9. Raichle ME et al (1983) Brain blood flow measured with intravenous H2(15)O. II. Implementation and validation. J Nucl Med 24(9):790–798
10. Ohta S et al (1996) Cerebral [15O]water clearance in humans determined by PET: I. Theory and normal values. J Cereb Blood Flow Metab 16(5):765–780
11. Gjedde A (1981) High- and low-affinity transport of D-glucose from blood to brain. J Neurochem 36(4):1463–1471
12. Ter-Pogossian MM et al (1970) The measure in vivo of regional cerebral oxygen utilization by means of oxyhemoglobin labeled with radioactive oxygen-15. J Clin Invest 49 (2):381–391

13. Ohta S et al (1992) Oxygen consumption of the living human brain measured after a single inhalation of positron emitting oxygen. J Cereb Blood Flow Metab 12(2):179–192
14. Sokoloff L et al (1977) The [^{14}C]deoxyglucose method for the measurement of local cerebral glucose utilization: theory, procedure, and normal values in the conscious and anesthetized albino rat. J Neurochem 28(5):897–916
15. Gjedde A (1982) Calculation of cerebral glucose phosphorylation from brain uptake of glucose analogs in vivo: a re-examination. Brain Res 257(2):237–274
16. Gjedde A et al (1985) Comparative regional analysis of 2-fluorodeoxyglucose and methylglucose uptake in brain of four stroke patients. With special reference to the regional estimation of the lumped constant. J Cereb Blood Flow Metab 5(2):163–178
17. Reivich M et al (1979) The [^{18}F]fluorodeoxyglucose method for the measurement of local cerebral glucose utilization in man. Circ Res 44 (1):127–137
18. Bass L et al (2011) Analogue tracers and lumped constant in capillary beds. J Theor Biol 285(1):177–181
19. Hasselbalch SG et al (2001) The [^{18}F]fluorodeoxyglucose lumped constant determined in human brain from extraction fractions of [^{18}F] F-fluorodeoxyglucose and glucose. J Cereb Blood Flow Metab 21(8):995–1002
20. Kuwabara H, Evans AC, Gjedde A (1990) Michaelis-Menten constraints improved cerebral glucose metabolism and regional lumped constant measurements with [^{18}F]fluorodeoxyglucose. J Cereb Blood Flow Metab 10 (2):180–189
21. Garnett ES, Firnau G, Nahmias C (1983) Dopamine visualized in the basal ganglia of living man. Nature 305(5930):137–138
22. Gjedde A et al (1991) Dopa decarboxylase activity of the living human brain. Proc Natl Acad Sci U S A 88(7):2721–2725
23. Kumakura Y et al (2005) PET studies of net blood-brain clearance of FDOPA to human brain: age-dependent decline of [^{18}F]fluorodopamine storage capacity. J Cereb Blood Flow Metab 25(7):807–819
24. Wagner HN Jr et al (1983) Imaging dopamine receptors in the human brain by positron tomography. Science 221(4617):1264–1266
25. Wong DF et al (1984) Effects of age on dopamine and serotonin receptors measured by positron tomography in the living human brain. Science 226(4681):1393–1396
26. Wong DF et al (1997) Quantification of neuroreceptors in the living human brain: III. D2-like dopamine receptors: theory, validation, and changes during normal aging. J Cereb Blood Flow Metab 17(3):316–330
27. Wong DF, Gjedde A, Wagner HN Jr (1986) Quantification of neuroreceptors in the living human brain. I. Irreversible binding of ligands. J Cereb Blood Flow Metab 6(2):137–146
28. Wong DF et al (1986) Quantification of Neuroreceptors in the living human brain. II. Inhibition studies of receptor density and affinity. J Cereb Blood Flow Metab 6(2):147–153
29. Gjedde A, Wong DF (2001) Quantification of neuroreceptors in living human brain. v. endogenous neurotransmitter inhibition of haloperidol binding in psychosis. J Cereb Blood Flow Metab 21(8):982–994
30. Mintun MA et al (1984) A quantitative model for the in vivo assessment of drug binding sites with positron emission tomography. Ann Neurol 15(3):217–227
31. Farde L et al (1986) Quantitative analysis of D_2 dopamine receptor binding in the living human brain by PET. Science 231(4735):258–261
32. Gjedde A et al (2005) Mapping neuroreceptors at work: on the definition and interpretation of binding potentials after 20 years of progress. Int Rev Neurobiol 63(1):1–20
33. Kuhar MJ et al (1978) Dopamine receptor binding in vivo: the feasibility of autoradiographic studies. Life Sci 22(2):203–210
34. Innis RB et al (2007) Consensus nomenclature for in vivo imaging of reversibly binding radioligands. J Cereb Blood Flow Metab 27 (9):1533–1539
35. Wong DF et al (1997) Quantification of neuroreceptors in the living human brain: IV Effect of aging and elevations of D_2-like receptors in schizophrenia and bipolar illness. J Cereb Blood Flow Metab 17(3):331–342
36. Wong DF et al (1998) Quantification of extracellular dopamine release in schizophrenia and cocaine use by means of TREMBLE. In: Carson RE, Herscovitch P, Daube-Witherspoon ME (eds) Quantitative functional brain imaging with positron emission tomography, 1st edn. Academic, San Diego, pp 463–468
37. Gjedde A et al (2010) Inverted-U-shaped correlation between dopamine receptor availability in striatum and sensation seeking. Proc Natl Acad Sci U S A 107(8):3870–3875
38. Koepp MJ et al (1998) Evidence for striatal dopamine release during a video game. Nature 393(6682):266–268
39. Wong DF et al (2006) Increased occupancy of dopamine receptors in human striatum during cue-elicited cocaine craving. Neuropsychopharmacology 31(12):2716–2727

40. Wong DF et al (2008) Mechanisms of dopaminergic and serotonergic neurotransmission in Tourette syndrome: clues from an in vivo neurochemistry study with PET. Neuropsychopharmacology 33(6):1239–1251
41. Laruelle M, Abi-Dargham A (1999) Dopamine as the wind of the psychotic fire: new evidence from brain imaging studies. J Psychopharmacol 13(4):358–371
42. McConathy J, Kilts CD, Goodman MM (2001) Radioligands for PET and SPECT imaging of the central noradrenergic system. CNS Spectr 6(8):704–709
43. Scott DJ et al (2007) Time-course of change in [^{11}C]carfentanil and [11C]raclopride binding potential after a nonpharmacological challenge. Synapse 61(9):707–714
44. Maarrawi J et al (2007) Motor cortex stimulation for pain control induces changes in the endogenous opioid system. Neurology 69 (9):827–834
45. Laruelle M et al (1997) Imaging D_2 receptor occupancy by endogenous dopamine in humans. Neuropsychopharmacology 17(3):162–174
46. Yokoi F et al (2002) Dopamine D_2 and D_3 receptor occupancy in normal humans treated with the antipsychotic drug aripiprazole (OPC 14597): a study using positron emission tomography and [^{11}C]raclopride. Neuropsychopharmacology 27(2):248–259

http://www.springer.com/978-1-61779-988-4

Molecular Imaging in the Clinical Neurosciences
Gründer, G. (Ed.)
2012, XII, 400 p. 119 illus., 48 illus. in color., Hardcover
ISBN: 978-1-61779-988-4
A product of Humana Press